On validating predictions of plant motion in coupled biomechanical-flow models

TIMOTHY I. MARJORIBANKS (IAHR Member), Postdoctoral Research Associate, *Department of Geography, Durham University, Lower Mountjoy, South Road, Durham. DH1 3LE, UK*

Email: tim.marjoribanks@durham.ac.uk (author for correspondence)

RICHARD J. HARDY (IAHR Member), Reader, *Department of Geography, Durham University, Lower Mountjoy, South Road, Durham. DH1 3LE, UK*

Email: r.j.hardy@durham.ac.uk

DANIEL R. PARSONS, Professor, *Department of Geography, Environment and Earth Sciences, University of Hull, Hull, HU6 7RX, UK*

Email: d.parsons@hull.ac.uk

Running Head: Validating plant motion models

On validating predictions of plant motion in coupled biomechanical-flow models

ABSTRACT

Recent developments in integrated biomechanical-flow models have enabled the prediction of the influence of vegetation on the flow field and associated feedback processes. However, to date, such models have only been validated on the hydraulic predictions and/or mean plant position. Here we introduce an approach where dynamic surrogate plant motion, measured directly in flume experiments, is used to allow a validation approach capable of assessing the accuracy of time-dependent flow-vegetation interaction within a numerical model. We use this method to demonstrate the accuracy of an existing Euler-Bernoulli beam model in predicting both mean and dynamic plant position through time and space.

Keywords: Biomechanics; flow visualization and imaging; Large Eddy Simulations; Particle Image Velocimetry; vegetated flows

1 Introduction

Integrated biomechanical and Computational Fluid Dynamics (CFD) flow modelling provides a methodology for studying complex flows through vegetation canopies, due to its ability to predict the whole-field relating to both flow and plant motion. However, the application of such models requires an assessment of their ability to reliably predict both flow variables and plant motion. Such validation is challenging due to difficulties in obtaining high quality, high-resolution flow and plant position data simultaneously within the flume or field environment. To date, validation has focused on an accurate prediction of the flow field (Marjoribanks, Hardy, Lane, & Parsons, 2014b) and mean plant height or plant position (Abdelrhman, 2007; Dijkstra & Uittenbogaard, 2010; Li & Xie, 2011; Mattis, Dawson, Kees, & Farthing, 2015).

Validating dynamic plant motion or applying a simultaneous validation of flow and plant motion is more problematic. To date, the only laboratory study to capture both flow and plant data is that of Okamoto and Nezu (2009). They developed a joint Particle Image Velocimetry (PIV)-Particle Tracking Velocimetry (PTV) methodology, to track the motion of individual stem tips as well as the flow. Their method was based upon an occupied-area discriminator (Nezu & Azuma, 2004) which relied upon a distinguishable size difference between the flow seeding and vegetation. Here we present a methodology for extracting entire plant position data from PIV data and use it to validate the Euler-Bernoulli beam model of Marjoribanks et al., (2014b). Similar to the method of Okamoto and Nezu (2009) the method

relies only upon one set of PIV images. However, instead of using an occupied-area discriminator, we apply a range of pixel-scale image analysis methods in conjunction with proximity tests to map the vegetation position through time and space. Such an approach enables simultaneous validation of flow and whole plant position, increasing the confidence in the predictive ability of biomechanical-flow models of vegetated flows.

2 Biomechanical model validation methodology

2.1 Flume setup

In order to validate the biomechanical model, we conducted laboratory experiments with a flume that contained a single surrogate vegetation stalk of the type used by Marjoribanks et al. (2014b). A single stem was used to ensure the easy identification of the stem within the flow. The stalk, which was 0.10 m long and had a radius (r_P) of 0.0025 m, was placed on the centreline of a smooth bed flume (10 m x 1 m x 1 m) with a flow depth of 0.4 m. Experiments were conducted at two different stem Reynolds numbers, (R_d = 1400 and 2700) in order to calibrate and then validate the biomechanical model. Flow and plant motion data were captured using a charge-coupled device camera, which was positioned perpendicular to the flow. Images were captured for 60 s at 50 Hz over a field of view of 0.52 m by 0.33 m with a pixel resolution of 0.6 mm. PIV flow data were obtained using the processes outlined by Hardy et al. (2005), to produce a 2D velocity map across the field of view, at a resolution of 0.0038 m, with an uncertainty in the order of 0.003 ms^{-1}.

2.2 Plant motion capture

In order to extract the plant position and shape, the raw PIV camera images (Fig. 1a) are subject to a suite of image analysis. Initially, the PIV image is converted to a binary mask (Fig. 1b) by applying a global thresholding process based upon the image luminance (Hardy, Best, Parsons, & Keevil, 2011). Selection of the threshold value is dependent on the surrogate and seeding material and must be chosen for the particular flume setup by manually calculating the minimum luminance value along the stem in a sample PIV image. As flume lighting conditions do not change significantly between images, this threshold remains constant throughout each experiment. The plant motion capture process is insensitive to small variations in this threshold.

Using the binary mask the images are further processed to refine the plant structure data and remove unwanted fluid seeding data. These binary techniques work on a pixel scale and alter the value of each pixel based upon the values of the proximal 8 cells. In particular, three specific algorithms are used: i) the first removes all isolated pixels; ii) the second

removes spurs within the data; and iii) finally the pixel value based on the mode of the proximal cells is calculated (Gonzalez, Woods, & Eddins, 2004). Each technique is repeated multiple times to improve the image. As with the luminance thresholding process, the exact selection of averaging methods and number of repetitions can be fine-tuned between datasets to account for differences in plant complexity, flume lighting and PIV seeding characteristics. However, this calibration is only necessary once per experimental dataset (~3000 images). Here we applied algorithms (i) and (ii) four times each followed three iterations of algorithm (iii).

Once the images have been analysed, an array of stem-centre points are identified (Fig. 1c), based upon horizontal and vertical averaging. Incorrectly identified plant data points, due to the interference of seeding material, were eliminated by subjecting the points to two final proximity tests. The first excluded points that were not within a fixed distance (5 pixels, 3 mm) of any other plant position points. This distance was chosen to eliminate points with separation greater than the stem radius (r_P). The second excluded points for which the sum of the distances between the closest twenty neighbours was greater than two median absolute deviations from the median of the equivalent sum over all plant position points. This was effective in removing small clusters of points associated with seeding within the flow. The final stem-centre points can be plotted to show the overall shape of the plant, or interpolated to achieve an equation for the stem shape. In this case, we use the entire plant shape to calibrate the numerical flow model parameters. For the validation of the biomechanical model, we extract the tip of the stem for analysis, as this produces an easily comparable time series. This process was fully automated and the final canopy height time-series was despiked to remove unphysical instantaneous spikes caused by errors within the automated process.

2.3 Numerical model setup

The experimental conditions were replicated in the integrated biomechanical-CFD model of Marjoribanks et al. (2014). A model domain 0.2 m long, 0.05 m wide and 0.2 m high was created, with a single vegetation stem placed along the centre line. The grid resolution in each direction was 0.001 m. Flow was simulated using Large Eddy Simulation with a Smagorinsky sub-grid model (C_S=0.17). A no-slip boundary condition was used at the bed while the walls were represented by frictionless boundaries. The free-surface was modelled using the rigid-lid approximation. The inlet conditions were taken directly from the PIV data, at the corresponding distance upstream from the stalk and interpolated onto the finer numerical grid. Further details regarding the numerical model can be found in Marjoribanks et al. (2014). The vegetation was simulated using the Euler-Bernoulli beam model, modified to account for an

initial radius of curvature ($r_c = 0.2$ m) within the stem. As the initial curvature was small ($r_c \approx 80 r_p$), the beam was solved from the initial curved position, under the assumption of a linear stress distribution across each beam cross-section (Kaplan, 1954; Timoshenko, 1955). The drag force acting on the stem was calculated directly from the pressure (Marjoribanks, Hardy, Lane, & Parsons, 2014a).

2.4 Analysis methods

In order to calibrate and validate the plant position data, we apply two techniques in addition to the bulk measures of the mean and standard deviation of plant height. First, we apply spectral analysis to assess the representation of different frequencies of motion both in the plant motion and within the flow. For this method, we use Welch's (1967) periodogram method with five non-overlapping intervals and a rectangular window to remove the effects of noise. Secondly, we apply wavelet analysis, as detailed in Marjoribanks et al. (2014b), which permits investigation of the time-varying periodicities in plant motion, across a range of frequencies.

2.5 Calibration of flexural rigidity

Flexural rigidity was initially calculated using bending tests as EI=0.0003 Nm^2. However, this value did not account for initial stem curvature. Therefore, the value of EI had to be calibrated using data from the experiments at R_d=1400. For this calibration, the mean velocity profile was used to ensure the stem reached an equilibrium position, and therefore the converged steady-state plant position within the simulation was compared to the distribution of experimental plant positions. This distribution of experimental positions was obtained by plotting the stem-centre position using a binary mask at each time step cumulatively to build up a map of plant occupancy (Fig. 2). This pixel-scale cumulative occupancy map shows a relatively steady plant position at this Reynolds number, with small scale plant motion evident from the increasing width of the area commonly occupied towards the top half of the stem (Fig. 2, inset).

An iterative calibration process resulted in a value of EI=0.000216 Nm^2 with the resulting numerical plant position shown by the red crosses in Fig. 2. Sparsity of experimental data due to the bottom fixing of the stem to the flume bed (See Fig. 1) and partial illumination of the left-hand edge of the stem within the bottom 0.03 m explains the greater discrepancy between the observed and simulated stem-centre within this region. Nevertheless, agreement is still good in this region with an error of less than 0.0015 m between the observed stem position and that obtained from the model.

3 Results

Validation of predicted plant position through time was conducted for the R_d=2700 case. In order to compare the data, full time series of stem height were extracted from both the flume and CFD data. The simulated mean and standard deviation of plant height for this case (Table 1) show less than 1.5% error in the mean and 10% error in the standard deviation from the measured value demonstrating the ability of the model to predict both the mean plant position and dynamic plant motion accurately.

The power spectra of plant height from the experiments and simulations (Fig. 3) are similar, particularly for the lower frequency end of the spectra. The time series data (Fig. 4a) demonstrate visually this similarity, most notably at the lower frequencies, between the flume and CFD data. The PIV data contain noticeably more large magnitude spikes within the time series. The despiking process only removed non-physical spikes that could be definitely categorised as those caused by erroneous identification of seeding (less than 5% of the data points). It is likely, given their sharp gradients, that some of the remaining spikes do correspond to the influence of seeding within the PIV images. There are clear time periods for which the numerical and experimental data show excellent agreement (e.g. ~41-46 s), as well as periods where large discrepancies appear (e.g. 12-14 s, 34-36 s). We suggest that as they contain a smooth underlying signal, these more persistent discrepancies relate to discrepancy in model prediction rather than error in the plant motion capture methodology.

The wavelet spectra (Fig. 4b-c) highlight periodicities within the flow for both the experimental and numerical data. The numerical data (Fig. 4b) show a particularly regular periodicity just below the 10 second scale, though this appears to split into two separate scales after approximately 25 s. The numerical data also highlight another distinct periodicity at an approximate 2 s scale, though this is less well defined and its scale appears to vary more through the time series. Both these identified scale ranges are also present within the experimental data (Fig. 4c), where there is periodicity at approximately 10 s scale, though this is less well defined than within the numerical data. Similar to the numerical data, this periodicity appears to split into two distinct scales with time. The smaller (~2 s) time-scale periodicity contains more power within the experimental data than the numerical data as evidenced by regions of high power and a more consistent periodicity throughout the time series.

The wavelet cross-spectrum (Fig. 4c) illustrates the regions of common power between the two datasets and confirms the trend seen in Fig. 3 and visually identified in Fig. 4a, whereby there is agreement between the two datasets across the scale range but there is greater similarity between the data at the lower frequencies. This is evident by the higher cross-wavelet power within the 5-10 s scale range. Across other scales, there is still

agreement, with the 2 s scale periodicity clearly identifiable within Fig. 4d. In summary, despite some variation, these results suggest that the biomechanical model is reproducing plant motion across a range of different scales.

4 Discussion

The results demonstrate the usefulness in applying an automated plant motion capture process in order to validate biomechanical models within a CFD framework. The low computational cost process presented here was able to produce whole-plant position data with mm-scale accuracy using only the original PIV images.

However, we acknowledge there are several limitations to the current method. Firstly, the technique requires an unobstructed view of the plant from the PIV camera and therefore would not be applicable to plants within a canopy. Secondly, the current method is only applicable to a single-stemmed plant. We are currently developing the method to help extract more complex plant forms, such as real aquatic macrophytes where tracking the plant tips is not sufficient to fully capture plant structure and variation. Such a development requires an adjustment of the threshold values as well as an advanced method of averaging the calculated stem points (Fig. 1b) to determine stem centres (Fig. 1c).

Thirdly, although the thresholding and proximity testing process was optimised to minimise the error, we still observed instances where seeding particles within the immediate proximity of the stem were included within the stem position. The automation process could be refined further to increase the accuracy and diminish erroneous points by setting a limit on identified stem widths to remove seeding close to the stem. This may remove some of the spikes within the data in Fig. 4. However, the advantage of this current method is that it provides a very fast, efficient method of collecting model validation data with low computational cost. This is ideal for extracting data from large time series of PIV images and in comparison to the method of Okamoto and Nezu (2009) is able to extract whole-plant positions rather than stem tips.

Using the plant motion capture process, validation of the plant motion for the Euler-Bernoulli beam model (Marjoribanks, et al., 2014b) shows that the model performs well at predicting both mean plant height and dynamic variation to plant posture. The model's predictive capability at lower frequencies is particularly important as canopy shear layer turbulence frequencies, not observed within this study, are typically of the order of 5-20 s scale (e.g. Ackerman & Okubo, 1993; Ghisalberti & Nepf, 2002; Okamoto & Nezu, 2009) and therefore will be represented accurately within this model. However, the results also indicate that the model performs well in reproducing the higher frequency (short time scale) oscillations that might correspond to plant-induced natural frequency vibrations (0.2-2 s). There are some instances where the match-up between the numerical and experimental data is

poor and further work is required to ascertain whether these errors relate to the plant motion capture methodology or unrepresented complexities within the flow-vegetation coupling.

5 Conclusions

This paper presents a simple image-analysis based procedure for extracting plant motion data from PIV images. This method has been shown to work well for single stems and needs to be developed for application to more complex canopy flows. However, the results demonstrate its applicability in validating integrated LES-biomechanical models such as those presented by Marjoribanks et al. (2014b). Validation of the Euler-Bernoulli model using this methodology reveals the accuracy of model in predicting both mean and dynamic plant position.

Acknowledgements

The authors wish to thank Dr Gareth Keevil, the experimental officer at Sorby Environmental Fluid Dynamics Laboratory, University of Leeds for his assistance with the flume experiments. The authors would like to thank the editor, associate editor and three anonymous referees whose comments have improved this manuscript. Data presented in this paper can be obtained by contacting the first author.

Funding

The first author was funded under a NERC PhD studentship and NERC Grant NE/K003194/1. The flume experiments were funded through UK NERC grant NE/ F010060/1.

Notation

C_S = Smagorinsky constant (-)
EI = flexural rigidity (Nm^2)
R_d = Stem Reynolds number (-)
h_v = vegetation height (m)
r_c = stem radius of curvature (m)
r_p = plant radius (m)
x = downstream coordinate (m)
z = vertical coordinate (m)
Σ = Cumulative pixel occupancy (-)

References

Abdelrhman, M. A. (2007). Modeling coupling between eelgrass Zostera marina and water flow. *Marine Ecology Progress Series, 338*, 81-96. doi:10.3354/meps338081

Ackerman, J. D., & Okubo, A. (1993). Reduced Mixing in a Marine Macrophyte Canopy. *Functional Ecology, 7*(3), 305-309. doi:10.2307/2390209

Dijkstra, J. T., & Uittenbogaard, R. E. (2010). Modeling the interaction between flow and highly flexible aquatic vegetation. *Water Resources Research, 46*(12), W12547. doi:10.1029/2010wr009246

Ghisalberti, M., & Nepf, H. M. (2002). Mixing layers and coherent structures in vegetated aquatic flows. [Article]. *Journal of Geophysical Research-Oceans, 107*(C2), 11. doi:10.1029/2001jc000871

Gonzalez, R. C., Woods, R. E., & Eddins, S. L. (2004). *Digital image processing using MATLAB*: Pearson Education India.

Hardy, R. J., Best, J. L., Parsons, D. R., & Keevil, G. M. (2011). On determining the geometric and kinematic characteristics of coherent flow structures over a gravel bed: a new approach using combined PLIF-PIV. *Earth Surface Processes and Landforms, 36*(2), 279-284. doi:10.1002/esp.2118

Hardy, R. J., Lane, S. N., Lawless, M. R., Best, J. L., Elliott, L., & Ingham, D. B. (2005). Development and testing of a numerical code for treatment of complex river channel topography in three-dimensional CFD models with structured grids. *Journal of Hydraulic Research, 43*(5), 468-480.

Kaplan, A. (1954). *Finite deflections and buckling of slightly curved beams and shallow spherical shells undeer lateral loads.* PhD, California Institute of Technology.

Li, C. W., & Xie, J. F. (2011). Numerical modeling of free surface flow over submerged and highly flexible vegetation. *Advances in Water Resources, 34*(4), 468-477. doi:10.1016/j.advwatres.2011.01.002

Marjoribanks, T. I., Hardy, R. J., Lane, S. N., & Parsons, D. R. (2014a). Dynamic drag modeling of submerged aquatic vegetation canopy flows. In A. J. Schleiss, G. De Cesare, M. J. Franca & M. Pfister (Eds.), *River Flow 2014*. London: Taylor and Francis.

Marjoribanks, T. I., Hardy, R. J., Lane, S. N., & Parsons, D. R. (2014b). High-resolution numerical modelling of flow—vegetation interactions. *Journal of Hydraulic Research, 52*(6), 775-793. doi:10.1080/00221686.2014.948502

Mattis, S. A., Dawson, C. N., Kees, C. E., & Farthing, M. W. (2015). An immersed structure approach for fluid-vegetation interaction. *Advances in Water Resources, 80*(0), 1-16. doi:10.1016/j.advwatres.2015.02.014

Nezu, I., & Azuma, R. (2004). Turbulence Characteristics and Interaction between Particles and Fluid in Particle-Laden Open Channel Flows. *Journal of Hydraulic Engineering, 130*(10), 988-1001. doi:10.1061/(ASCE)0733-9429(2004)130:10(988)

Okamoto, T. A., & Nezu, I. (2009). Turbulence structure and "Monami" phenomena in flexible vegetated open-channel flows. *Journal of Hydraulic Research, 47*(6), 798-810. doi:10.3826/jhr.2009.3536

Timoshenko, S. (1955). *Strength of Materials* (3rd ed. Vol. 1). New York: D. Van. Nostrand Company, Inc.

Welch, P. (1967). The use of fast Fourier transform for the estimation of power spectra: A method based on time averaging over short, modified periodograms. *Audio and Electroacoustics, IEEE Transactions on, 15*(2), 70-73.

Table 1 Stalk height statistics for the PIV and CFD data at R_d=2700

Dataset	Mean (m)	Standard Deviation (m)
PIV	0.0655	0.0032
CFD	0.0654	0.0029

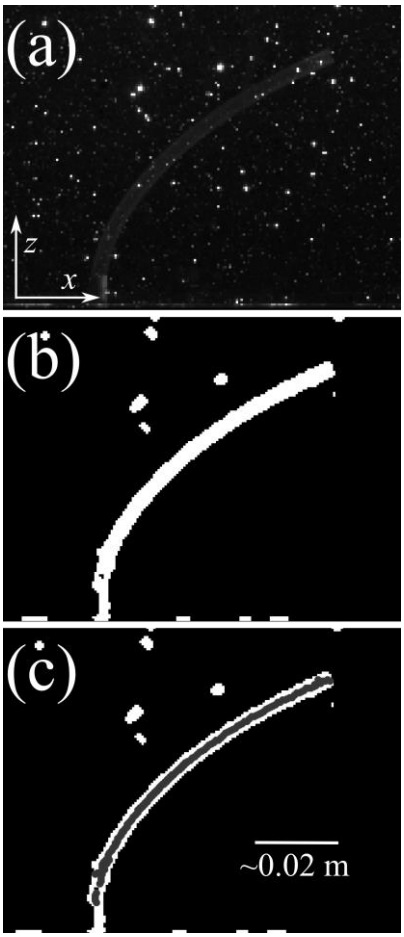

Figure 1 Plant motion capture methodology. Here, raw PIV images (a) are filtered and analysed to isolate the stalk from the flow (b). The stem centre points are then calculated (c). Flow is from left to right.

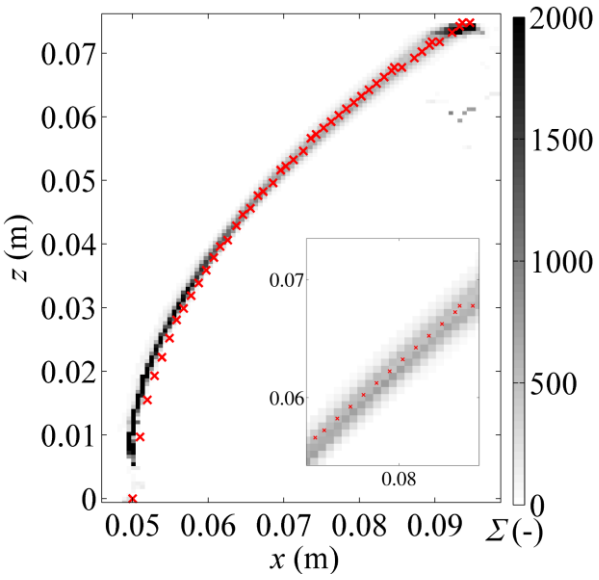

Figure 2 Comparison between experimental plant position and simulated mean plant position for the R_d=1400 case. Experimental plant position occupancy is shown in greyscale, with darker regions showing greater occupancy by the vegetation within those pixels. The simulated plant position is denoted by red crosses. The inset figure shows a close up of one plant section.

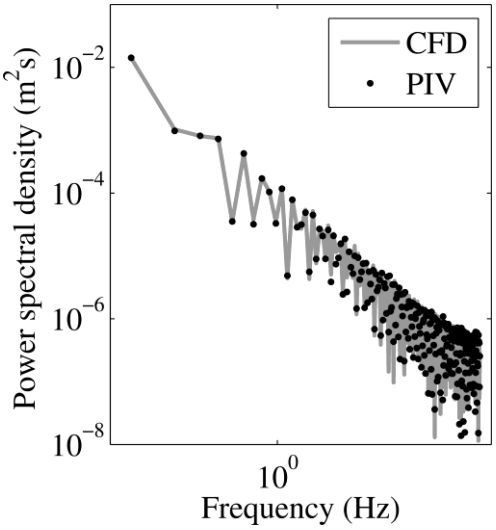

Figure 3 Power spectra for the PIV (black) and CFD (grey) time series of plant height. For the PIV data, only discrete data points are plotted for clarity.

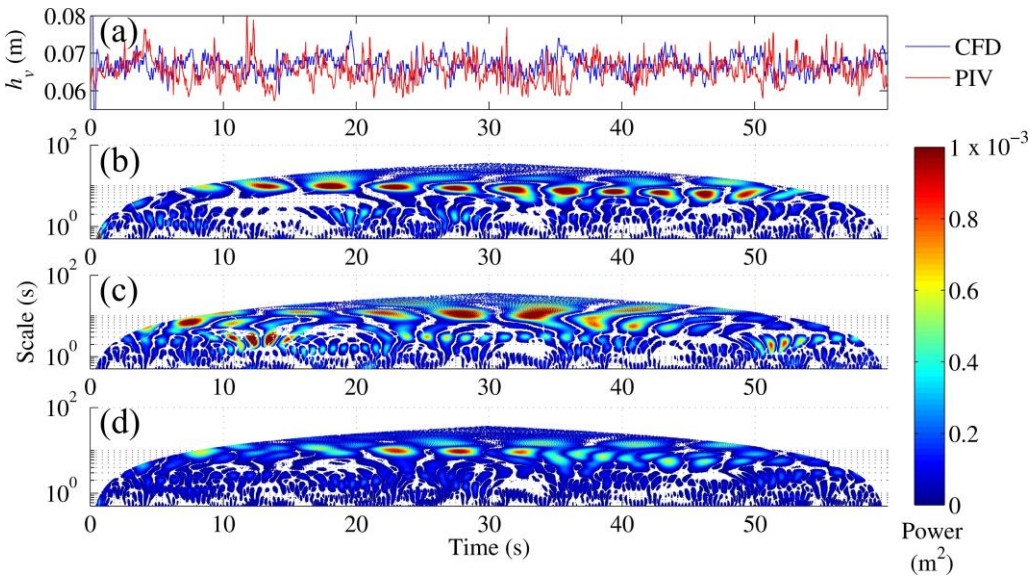

Figure 4 Time series (a) and wavelet spectra for the CFD (b) and PIV (c) plant height data. The cross-wavelet spectra between the CFD and PIV data is shown in (d).Regions of white in figures (c-d) represent areas of no statistically significant wavelet power.